Journal of Alloys and Compounds 639 (2015) 659–668

Contents lists available at ScienceDirect

Journal of Alloys and Compounds

journal homepage: www.elsevier.com/locate/jalcom

Microstructure evolution of thermal spray WC–Co interlayer during hot filament chemical vapor deposition of diamond thin films

Taimin Yang [a], Qiuping Wei [a,b,*], Yao Qi [a], Yijia Wang [a], Youneng Xie [a], Jiaqi Luo [a], Zhiming Yu [a,*]

[a] School of Materials Science and Engineering, Central South University, Changsha 410083, PR China
[b] State Key Laboratory of Powder Metallurgy, Central South University, Changsha 410083, PR China

ARTICLE INFO

Article history:
Received 10 December 2014
Received in revised form 13 March 2015
Accepted 17 March 2015
Available online 23 March 2015

Keywords:
Diamond film
HFCVD
WC–Co interlayer
HOVF
Diffusion
Phase transition

ABSTRACT

In this paper, diamond film was deposited on WC–Co coated steel substrate by hot filament chemical vapor deposition (HFCVD). This method can not only prepare diamond film on the sample, but also can be used as a new way of WC–Co coating heat treatment. Brittle phases, such as η phase, which were produced during ordinary heat treatment process, will be suppressed in HFCVD at high temperature. This paper systematically studied the microstructure (defects and phase) transition of WC–Co interlayer in the process of depositing diamond film. The mechanism of phase transition was discussed. The results showed that at high deposition temperature (e.g. 800 °C), the transition of binder phase was fast. After 5 h of deposition, the phase composition of WC–Co coating was almost the same as sintered WC–Co block. At low deposition temperature (e.g. 700 °C), the phase transition of interlayer slowed down and there was a large amount of nano-phases in the interlayer even after 12 h of deposition.

Another notable feature is that phase transition of the surface part of interlayer was the fastest, followed by the inner part and the middle part was the slowest. The phase transition rate of the interlayer and the binder phase is closely related to the depth of the coating. In the surface part of the coating, Co will evaporate and diffuse into diamond film. Also, activated carbon atoms will diffuse into the interlayer, but the depth of diffusion layer was limited. Fe and Co will diffuse into each other at the interface between interlayer and steel substrate. In contrast, the middle part of interlayer was not affected by diffusion of elements.

In sum, the results suggest that the change in element content (i.e. concentration diffusion) is the main driving force of the phase transition, while temperature mainly affects phase transition rate (i.e. the rate of diffusion).

1. Introduction

In the early 1990s, some scholars put forward ideas in preparing diamond coating on steel surface, but there was no significant breakthrough [1,2]. This is because the thermal expansion coefficient mismatch between steel and diamond is too large [2,3]. Temperature variation will generate large thermal stress [4,5]. Furthermore, iron is a catalyst for graphite and the solubility and diffusion rate of carbon in iron is high. During HFCVD process, a large number of carbon atoms will diffuse into steel substrate, which prolong the nucleation period. Also, graphite, amorphous carbon and other non-diamond phase will be produced on steel surface [6]. So the quality of diamond film is low.

From previous reports, the most effective approach is preparing high quality interlayers on steel surface. The interlayer will shield the adverse effects of substrate. By selecting suitable interlayers, the adverse effect of Fe can be avoided and the adhesion of diamond film will be stronger. There were dozens of interlayers reported [7–11]. But none of them was used in industrial scale production [12] because these interlayers cannot achieve effective mechanical and thermal transition between diamond and steel [13]. Metal interlayers can increase the nucleation density after seeding process [14–16] and the thermal expansion coefficient is close to steel, but it is much larger than diamond. So they cannot release thermal stress. Besides, metal interlayers will react with carbon atoms at high temperature, forming brittle carbides [17,18]. When it comes to ceramic interlayers, whose thermal expansion coefficient is larger than diamond and small than steel [17,19], they easily crack during HFCVD process due to poor toughness [20].

* Corresponding authors at: School of Materials Science and Engineering, Central South University, Changsha 410083, PR China (Q.P. Wei). Tel.: +86 731 8830335; fax: +86 731 8876692.
E-mail addresses: qpwei@csu.edu.cn (Q. Wei), zhiming@csu.edu.cn (Z. Yu).

http://dx.doi.org/10.1016/j.jallcom.2015.03.134
0925-8388/

In order to prepare abrasion-resistant diamond film on interlayer, WC–Co interlayer is prepared on steel using High-velocity Oxy-fuel thermal spraying technology (HVOF). However, compared with sintered WC–Co, the toughness, wear-resistance and erosion-resistance of WC–Co coating is much lower. This is because there are many kinds of defects in as-sprayed WC–Co coating, such as tiny pores, island boundaries, tungsten semi-carbide, γ phase and η phase. These defects and thermal dynamically unstable phases are produced during the thermal-spraying process, in which melted WC–Co drops were quenched when they reached the substrate. These defects and thermal dynamically unstable phases will deteriorate the performance of the coating. The phase distribution in the coating was not uniform, leading to large difference in mechanical and corrosion-resistant properties in different areas [21]. Many researchers found that W_2C will reduce the fracture toughness of the coating and decarbonized carbide phases is preferentially etched. For example, thermal-sprayed coatings normally contain non-uniform distributions of carbide and cobalt "lakes". The tribological behavior, abrasion and corrosion resistance of WC–Co coatings are generally poorer than sintered WC–Co. This indicates that the inhomogeneous microstructure and the phase transformations of the starting material, which can lead to wide variations in mechanical properties and in corrosion resistance [22]. Thakare et al. found that wear occurs by preferential removal of binder around the carbide grains exposing them to the abrasives which subsequently leads to their cracking and pull-out [23]. Lima et al. found that W_2C fraction seems to be the decisive element in the fracture toughness of WC–Co coatings and appropriate post-heat treatments can improve the indentation toughness of thermally sprayed WC–Co coatings [24].

Post-heat treatment under inert atmosphere can partially eliminate these defects and improve the mechanical performance of the coating [24,25]. Adequate post-heat treatments can lead to an increase in coating toughness. Under inert atmosphere, heat treatment above 600 °C results in significant phase changes within the coating. Heat treatment changed the integrity and residual stress state of the coating and heat treatment could improve the wear behavior. However, the temperature of the ordinary heat treatment process cannot be too high. Stewart found that heat treatment under high temperature produced large-scale cracks while heat treatment under low temperature created microcracks, which is beneficial to the abrasive wear resistance of the coating [25]. Kim found that the performance of the sample will be greatly deteriorated after inert atmospheric heat treatment above 800 °C. This is because η phase will precipitate in the coating during the treatment process [26]. Ghadami et al. studied the structural and oxidation behavior of WC–Co coatings in air atmosphere. Their results demonstrated that higher temperature will result in acceleration of oxidation, producing WO_3, $CoWO_4$, etc. Above 1100 °C, the coating later will detach from the substrate [27].

Previously, Wei found in their XRD results that poor-carbon phase in WC–Co coating will transform into WC during HFCVD process. Eventually, the phase composition of thermal-sprayed WC–Co interlayer will develop into sintered WC–Co [31,32]. They demonstrates that WC–Co coatings can be the most effective interlayer, simultaneously guaranteeing diamond film quality and good adhesion at both the substrate/interlayer and the interlayer/diamond film interfaces [31,32]. But they did not know why and overlooked the microstructure transition in the WC–Co coating. In this paper, diamond/WC–Co/steel composite coating system was investigated in detail. By adjusting CVD parameters, phase evolution of the interlayer under different temperature was systematically studied.

2. Experiment

The diamond films were grown on AISI 1085 carbon steel plates and a WC–Co coating was used as an interlayer to improve the nucleation, quality and adhesion of the diamond film. The flat specimens used in this study were $50 \times 30 \times 5$ mm^3 AISI 1085 carbon steel plates coated with a WC–Co interlayer (200 μm in thickness) by HVOF. WC powder and Co powder was bought from Zhuzhou Cemented Carbide Group Co., Ltd. The size distribution of WC and Co powder was 2–3 μm and 2–5 μm, respectively. WC powder and Co powder was agglomerated and sintered together into large sprayable granules. The WC–Co granule used here typically comprised 83% WC and 17% Co powder. The HVOF torch is made by Sulzer Metco and the model is wokastar-600. Kerosene is used as fuel. The spraying parameters were: oxygen flow 56.64 m^3/h; spray distance 30 cm; fuel rate 0.0227 m^3/h; traverse speed 2 m/s. The substrates were machined into smaller plates of dimension $7 \times 7 \times 5$ mm^3 by spark machining. The specimens were polished with diamond polishing agent. The final interlayer thickness after polishing was 100 μm and the Ra value was about 0.3 μm.

Next, the samples were treated by two-step chemical pretreatment to remove Co. The samples were etched by (I) Murakami reagent (10 g $K_3[Fe(CN)_6]$ + 10 g KOH + 100 mL H_2O) in ultrasonic bath for 3mins (II) Mixed acid (2 mL 96 wt.%H_2SO_4 + 2 mL 68 wt.%HNO_3 + 20 mL 40% H_2O_2 + 40 mL H_2O) in ultrasonic vessel for 2mins. All samples were submerged in nano-diamond ultrasonic bath for 15mins before they were sent into the HFCVD equipment, designed and constructed in the Department of Physics at the Royal Institute of Technology, Stockholm (Sweden).

Then, the samples were divided into two groups, A and B. Samples in group A were deposited at 800 °C for 5 h and 12 h. Samples in group B were deposited at 700 °C for 5 h, 12 h and 48 h. Other deposition parameters were the same: chamber pressure 3 kPa, CH_4 1.5 sccm, H_2 48.5 sccm. Specimens were characterized by a variety of techniques, including scanning electron microscopy (FEI, Quanta200 Environmental SEM and FEI NovaSEM 230), Electron Microprobe Analysis (JEOL, JXA-8230), X-ray diffraction (Dmax-2500 VBX using Cu Kα radiation at a wavelength of 0.154 nm, scan speed: 8 deg/min), energy dispersive X-ray analysis (EDS: EDAX model) and Raman spectroscopy (LabRAMHR800). Raman spectra were measured with an argon ion laser operating at 488 nm with an output power of 10 mW.

3. Result

3.1. Surface morphology of diamond film

Fig. 1 is the surface morphology of diamond film deposited at 800 °C. As can be seen from the figure, the samples have cauliflower-like surface, which is induced by the diffusion of cobalt. With the extension of deposition time, the cauliflower-like morphology tended to disappear and the diamond grains were bigger. Another notable feature is that there are some nanoparticles on the surface of diamond grain. From EDS results (see in supplementary data Fig. S1), these nanoparticles were comprised of Co. As growth time increases, these nanoparticles became smaller and graphite wrapped on the surface of diamond grain was reduced.

Fig. 2 is the surface morphology of diamond film deposited at 700 °C. As growth time increases, the surface morphology was similar to 800 °C. However, in magnified figures, no Co nanoparticles (NP) can be seen on the surface of diamond grains. In addition, the size of diamond grain was much smaller compared with samples processed at 800 °C within 5 h and 12 h. After 5 h growth, the size of most diamond grains was under 0.5 μm. When deposition time was extended to 12 h, the average size of diamond grains increased to 2 μm. As time increased to 48 h, the size can reach 20 μm.

3.2. Raman spectra of diamond film

Fig. 3 is Raman spectrum of samples after diamond deposition. In figure (a and b), the main peaks were located at 1332 cm^{-1} (diamond) and 1500 cm^{-1} (non-sp^3). Obviously, as time increased, non-sp^3 carbon was reduced significantly. Figure (c, d and e) demonstrate the Raman spectrum of diamond film deposited at 700 °C. The main peaks were located at 1332 cm^{-1} (diamond), 1500 cm^{-1} (non-sp^3) and 1600 cm^{-1} (non-sp^3). The deposition time was 5 h, the intensity of non-sp^3 peak of samples deposited

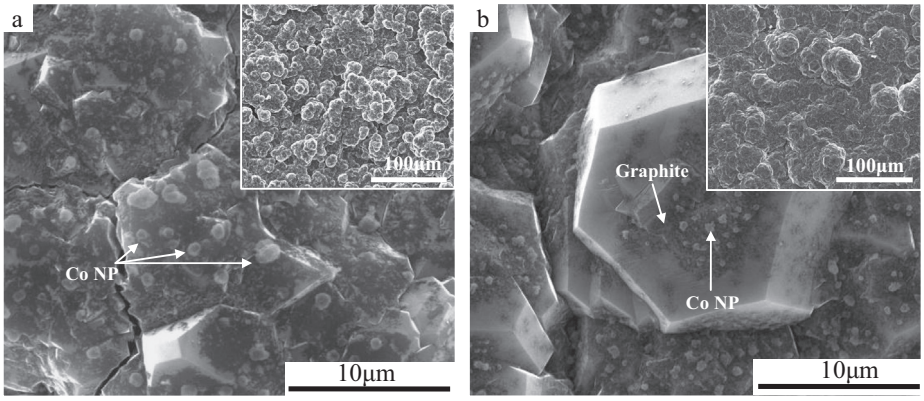

Fig. 1. Surface morphology of samples deposited at 800 °C in (a, c) 5 h; and (b, d) 12 h.

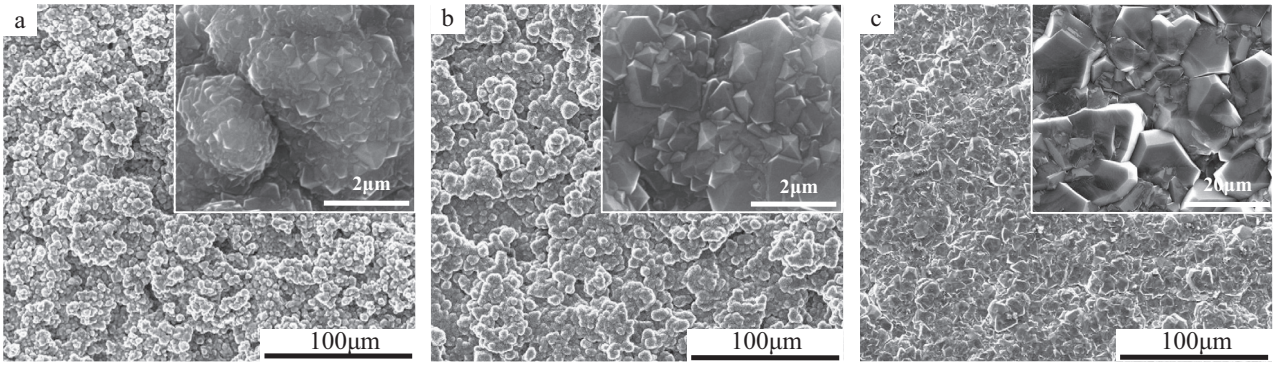

Fig. 2. Surface morphology of samples deposited at 700 °C in (a, d) 5 h; (b, e) 12 h; and (c, f) 48 h.

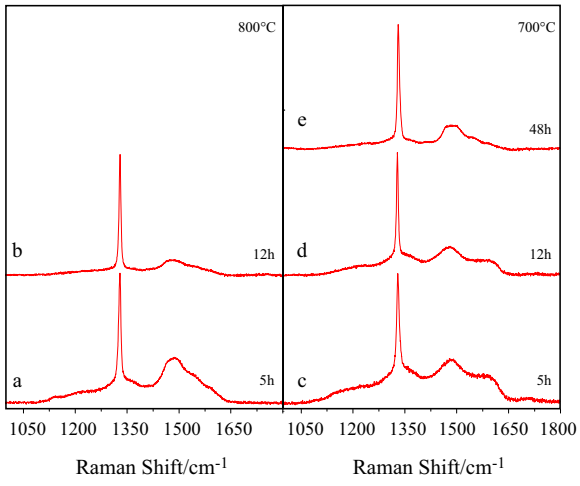

Fig. 3. Raman spectroscopy of samples deposited at 800 °C and 700 °C for 5 h, 12 h and 48 h.

at 700 °C and 800 °C was almost the same. Non-sp^3 carbon will also be reduced as growth time increases. When deposition time was extended to 12 h, the non-sp^3 peak of the sample deposited 800 °C is smaller. Overall, diamond film deposited at 800 °C has less non-sp^3 carbon and the quality is better.

3.3. XRD analysis

As can be seen from Fig. 4(a), the coating contained a large amount of amorphous phase because there is a broad peak located at 37–47° [28] and the intensity of XRD peak was not strong. The coating contained WC, W_2C, Co_2W_4C and $Co_3W_9C_4$.

After depositing diamond film at 700 °C and 800 °C for 5 h, notable changes appeared in the XRD pattern. Broad peaks located at $2\theta = 40°$ and $2\theta = 72°$ almost disappeared, except that there were low-intensity broad peaks in XRD of samples deposited at 700 °C. According to literature, these broad peaks represented amorphous phase containing W and Co [29]. After diamond deposition, most of nano phases and amorphous phases were crystallized. The variation of XRD pattern was concluded as follows: (1) The intensity of XRD peaks was much stronger and the noise in the patterns was much weaker (2) Amorphous broad peaks could not be observed (3) The amount of W_2C decreased rapidly. At 800 °C, Co_3W_3C peaks were found while at 700 °C the surface part of interlayer only contained small amount of W_2C and Co_2W_4C.

When deposition time was extended to 12 h and temperature remained at 800 °C, the XRD pattern is similar to the pattern of samples subjected to the 5 h deposition process, except that the intensity of XRD peaks is stronger. The intensity of the diamond peaks in the XRD pattern of the sample deposited at 700 °C for 12 h are also stronger than those seen after 5 h, but compared with samples deposited at 800 °C, the peaks are less intense because of lower thickness of the diamond film in the former case. The phase in the interlayer still contained W_2C and Co_2W_4C. At the same time, Co_3W_3C precipitated in the binder phase. This elucidates that high temperature will make it easier for the amorphous phase in the binder to crystallize. At 800 °C, after 5 h deposition, most of W_2C transformed into WC (will be proved in Section 3.5), while at 700 °C, there were still some amorphous phase in the interlayer after 12 h deposition.

After deposition at 700 °C for 48 h, in XRD pattern, the intensity of diamond peak exceeds WC peaks. There is no decarbonized

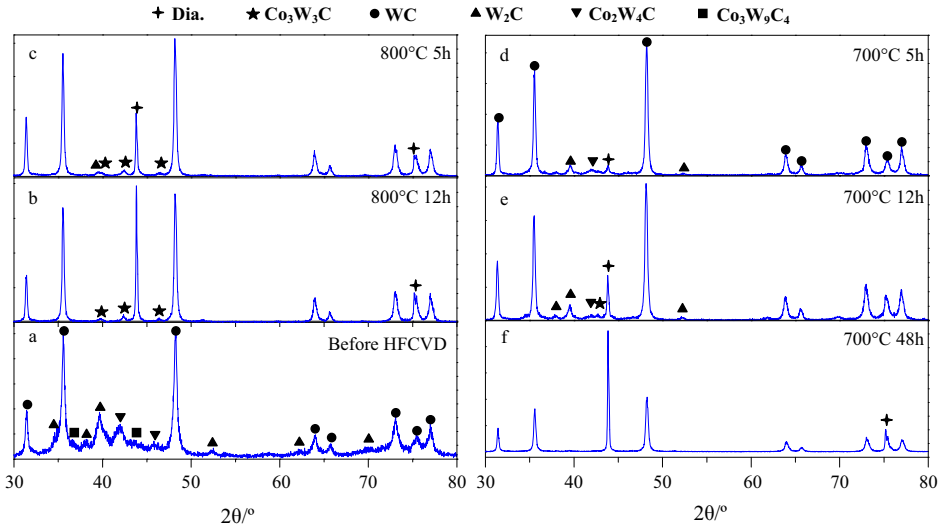

Fig. 4. X-ray diffraction patterns of samples (a) before deposition; (b, c) deposited at 800 °C in 12 h and 5 h; and (d, e, f) 700 °C in 5 h, 12 h and 48 h.

phase or Co-containing phase in the coating, which means that most of Co dissolved in nano-crystalline binder phases. According to previous reports, dendrite Co phase was found in specific areas in the coating, which was confirmed in the BSE images.

3.4. Microstructure analysis of as-sprayed WC–Co interlayer

Generally (Fig. 5a1), the brighter part is tungsten carbides and the darker part is binder containing Co. The size of tungsten carbides varies largely. Some of them can reach several micrometers and some can only reach a few hundred of nanometers. Most of grains have irregular shape and lose their edges during thermal spraying. Most of WC grains have no direct contact with each other and the volume of binder phase increases greatly compared with feedstock powder. In addition, there are a small number of pores in the coating, which were formed during thermal spraying.

Fig. 5(a2) is a magnified picture of Fig. 5(a1). From this picture, it can be seen that beside some of WC grains, some brighter phases appear. Some of them were dendrites and others were wrapped around WC grain. These phases are W_2C, which transformed from WC during HVOF thermal spraying. There were some dark, dispersed nanoparticles in the figure, which might be oxide inclusions. As can be seen from Fig. 5(a3), some parts of the coating were darker than the binder phase. In these areas, WC grains have regular shape and no W_2C can be found around WC grain. This elucidates that during thermal spraying powder is not heated evenly. The heating temperature of a small amount of powder is so low that WC cannot dissolve in Co binder phase, resulting in low W content in certain parts of the coating.

In Fig. 5(a2–a4), there were dispersed nanoparticles which were even brighter than W_2C. These were tungsten nanoparticles. Several dark lines can be found in these figures and nano-phases were distributed along these lines, which is called island boundary. According to Verdon's report [29], the content of W, C and O along island boundary is higher than binder phase and nano-sized W can be observed near island boundary. This is because the surface of powder particle has the highest temperature and oxygen density. Some WC was decarbonized into W, which is brighter. Island boundaries have negative influence on the mechanical performance of the coating. Therefore, island boundaries should be eliminated in order to improve the corrosion and wear resistance of the coating. The formation mechanism of island boundary is that WC–Co particles were heated during thermal spraying and Co can be heated to molten state. When heated particles reached the steel substrate, they were cooled rapidly and solidified on the surface of the substrate. Due to the uneven heat distribution during thermal spraying process, the temperature of some of molten particles is sufficient to melt the surface part of particles which already solidified. In this case, no island boundary can be found in the coating. If the temperature of molten particles cannot melt the surface of solidified particles, there will be island boundary between these particles.

In Fig. S2, EMPA analyzed four elements, i.e. C, W, Co, Fe. The analyzed section is WC–Co coating near steel substrate. As can be seen from the figure, C in binder phase is lower than WC grain. In areas where Co is high, content of carbon and tungsten is the lowest. Tungsten did not uniformly distribute inside WC grain. Before diamond deposition, the content of Fe in interlayer is as low as 0.835%.

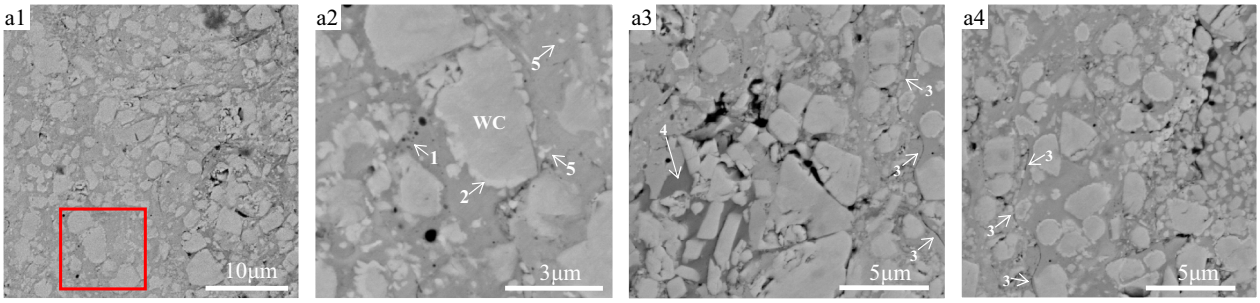

Fig. 5. (a) Back Scattering Electron (BSE) images. The numbers represent 1: oxide inclusions, 2: W_2C, 3: island boundary, 4: Co aggregated area and 5: tungsten nanoparticles.

3.5. WC–Co interlayer microstructure and element distribution after HFCVD

Figs. 6 and 7 are BSE images of samples after diamond deposition under different deposition parameters.

When parameters were set to 700 °C and 5 h (Fig. 6b), there were many similarities between the sample after diamond deposition and as-sprayed WC–Co interlayer. (1) Island boundaries in the middle part of interlayer; (2) a large number of nano-sized phases; (3) W_2C wrapped around the rim of WC grain; (4) Co aggregated in certain regions in the interlayer. Still there were some differences before and after diamond deposition. First, after diamond deposition, in the middle part of interlayer, W_2C around the rim of WC grain grew larger. Second, there was no obvious island boundary near the surface of interlayer and the average distance between each WC grains was smaller. In this region, nano-sized second phases with brighter contrast appeared in the binder. These phases were probably mixtures of W, W_2C and other W/Co/C phases.

When deposition parameters were set to 800 °C and 5 h (Fig. 6a), the most distinguishable difference was no island boundaries and Co-aggregated areas can be seen. Near the steel substrate, the number of pores in the coating increased and crevices can be found between WC grains and the binder phase. The distance between adjacent WC grains was even smaller and some of them grew into a large grain. Most of W_2C that wrapped around the WC grains disappeared. Inside WC grains, defects such as pores and cracks can be observed. In figure (a3, A3) which represented near-surface part of WC–Co coating, several WC grains aggregated into a larger grain. In addition, a large number of nanoparticles were distributed in certain regions in the binder phases. The aggregation of nanoparticles, according to existing literature [30], is γ phase. This phase is brittle. Due to the decrease in effective metallic binder, the existence of the γ phase in the coating is detrimental to the structure of the coating.

After HFCVD treatment at 700 °C for 48 h (Fig. 6c), inside the interlayer, island boundary disappeared. The contrast of binder phase was the same, meaning that the distribution of elements in the binder was uniform. Near the steel substrate, W_2C nanoparticles can be found around the rim of WC grains. Only a small fraction of W_2C can be observed in binder phase. In addition, there was large size difference between each WC grain. In the middle part of the interlayer, the content of W_2C was higher than other part of the interlayer. In this area, the distance between different grains was relatively large. In figure (c3, C3), near diamond film, there was no binder phase in the coating and average WC grain size was much larger.

After HFCVD of diamond film at 700 °C for 12 h (Fig. 7b), elongated splats (the molten or semi-molten particles impact on the substrate and form a laminar coating composed of many layers) and island boundary was found. Along island boundary, nano-sized particle phases were observed, which might be mixture of W, WC and W_2C. Similar to sample processed at 700 °C for 5 h, there were certain areas where the contrast was darker. Comparatively, near the surface, WC grains had tendency to aggregate. The distance between each grain was smaller and the amount of nanoparticles in the binder phase increased. Near the substrate, there were pores distributed in the WC–Co coating and creaks began to appear between grains and binder phase. In the middle part of the coating, there were some large WC grains, around which dendrite W_2C was found.

After diamond deposition at 800 °C for 12 h (Fig. 7a), similar to the sample deposited at 800 °C for 5 h, island boundary disappeared. There were tiny pores inside the binder phase and many WC grains. The distance between each WC grain was reduced. Nevertheless, γ phase were observed in the binder phase near steel substrate and in the middle of the coating. In the middle part of the coating, W_2C was found around the rim of WC grain. In the near-surface part of the coating, the aggregation of WC grains was even obvious. The shape of WC grains was regular and sharp corner appeared. But the binder phase between each WC grains was transformed, leaving large pores in the coating. This evolution will greatly reduce the toughness of the coating.

Fig. 8 presents EPMA images of HFCVD-processed samples, showing the element distribution of the cross-section of the coating. Fig. 8 showed element distribution of samples deposited at 700 °C for 5 h and 48 h. The analyzed areas were near the steel substrates. In Fig. 8(a4), Co aggregated in some regions. In Fig. 8(b2), near steel substrate, the concentration of C was higher compared with Fig. 8(a3). This is because near the substrate, there were many WC grains and the content of binder phase was low. Fe did not uniformly distribute in the interlayer and the average Fe mass ratio in the interlayer increased to 0.952%. As deposition time increased to 48 h, the mass ratio of Fe increased to 1.19%. This is because Fe in steel substrate diffused into WC–Co coating during HFCVD treatment. The mass ratio of C in the interlayer dropped from 1.54% to 1.3%, showing that C diffused into the steel substrate. After 48 h HFCVD, mass ratio of Co in the coating dropped from 16.22% to 15.59%. This means Co also diffused into the steel substrate during deposition process. There was no alteration in W mass ratio, meaning that at 700 °C, neither W in WC grain nor W in binder phase will diffuse into steel substrate.

4. Discussion

HFCVD process is very different from ordinary atmospheric heat treatment. In the reaction chamber of HFCVD, methane is decomposed and activated into active carbon atoms, which will diffuse into the surface of the substrate and encourage the formation of WC. Another notable feature of this process is that the temperature gradient in the reaction chamber is very large. Using HFCVD as a heat treatment approach can inhibit the formation of η phase in WC–Co coating and diamond film will grow on the surface of coating, which will greatly improve the wear-resistance and corrosion-resistance [33]. In addition, the island boundary in the coating will be eliminated under suitable deposition condition. Therefore, the attachment and toughness of the WC–Co layer will be greatly enhanced, as reported by Kim [26]. Moreover, W_2C around the rim of WC grain will be transformed into WC and the dissolved W will precipitate in the coating during HFCVD, forming W nanoparticles in the binder phase. Some W will transform into WC, which epitaxially grow around the WC grains, creating larger WC grains. The phase transition and microstructure evolution of WC–Co interlayer after HFCVD were discussed below.

4.1. Effect of temperature on phase transition of WC–Co coating

According to experimental results, temperature has great influence on evolution of island boundary and phase in WC–Co interlayer. After HFCVD at 800 °C for 5 h, the island boundary in the coating was blurring. Near steel substrate and diamond film, WC grains tended to aggregate. Only a small number of WC grains were wrapped by W_2C. After 12 h deposition, island boundary in the interlayer disappeared. This phenomenon is caused by the diffusion and crystallization of binder phase under elevated temperature. WC grains aggregation was more obvious near steel substrate and diamond film. W_2C can only be found in the middle part of the interlayer. By contrast, when substrate temperature was set to 700 °C, the evolution of coating was much slower. After 12 h deposition, Co still aggregated in certain parts of the coating and island boundaries were found. Near WC grains and island boundary, nano-sized phases were observed, which consisted of W,

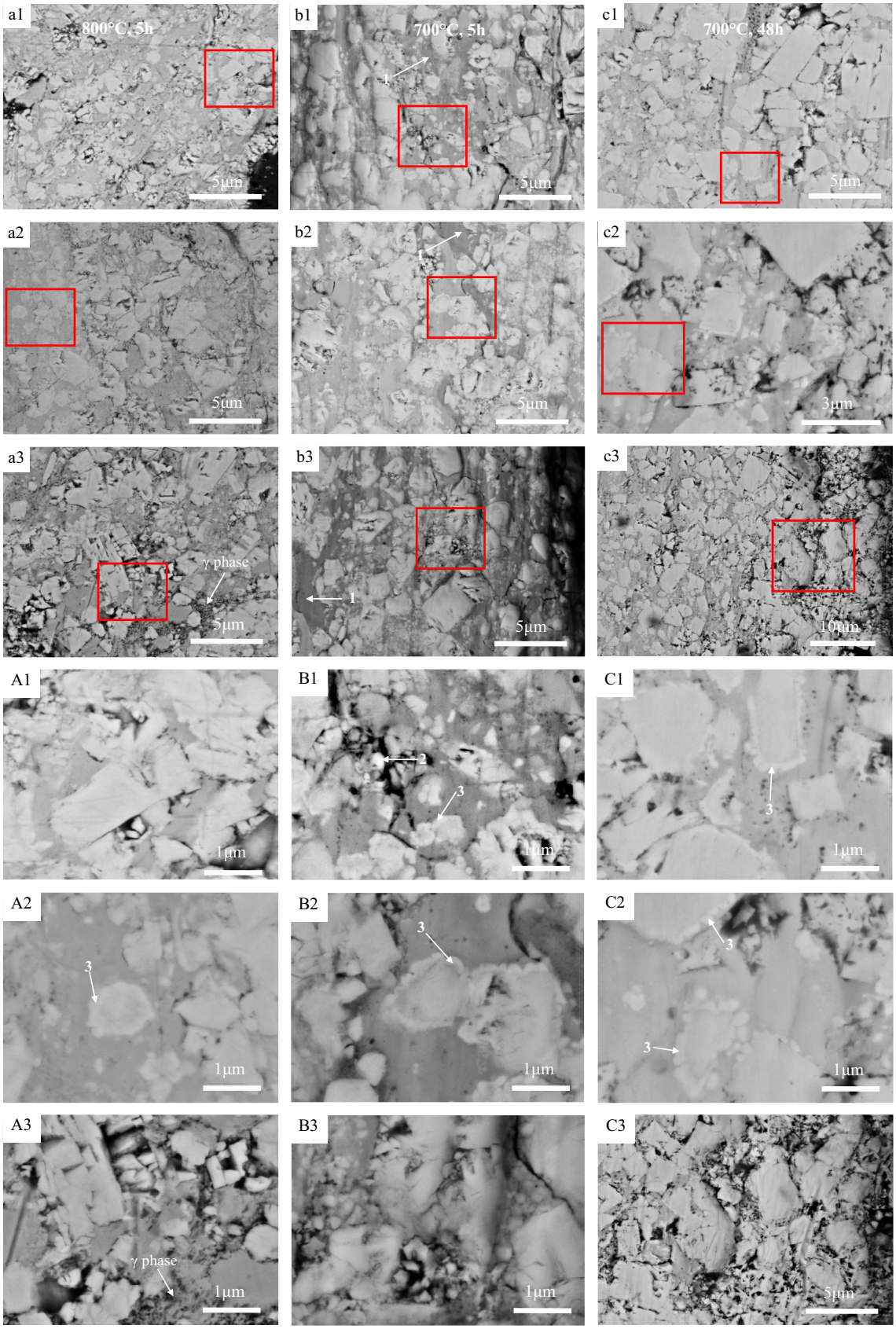

Fig. 6. Back Scattering Electron (BSE) images of the cross-section of samples deposited at (a) 800 °C in 5 h; (b) 700 °C in 5hours; (c) 700 °C in 48 h with different sites (1) near the steel substrate; (2) in the middle; (3) near the diamond film. Number 1 represents Co aggregated areas. Number 2 represents tungsten nanoparticles. Number 3 represents W_2C.

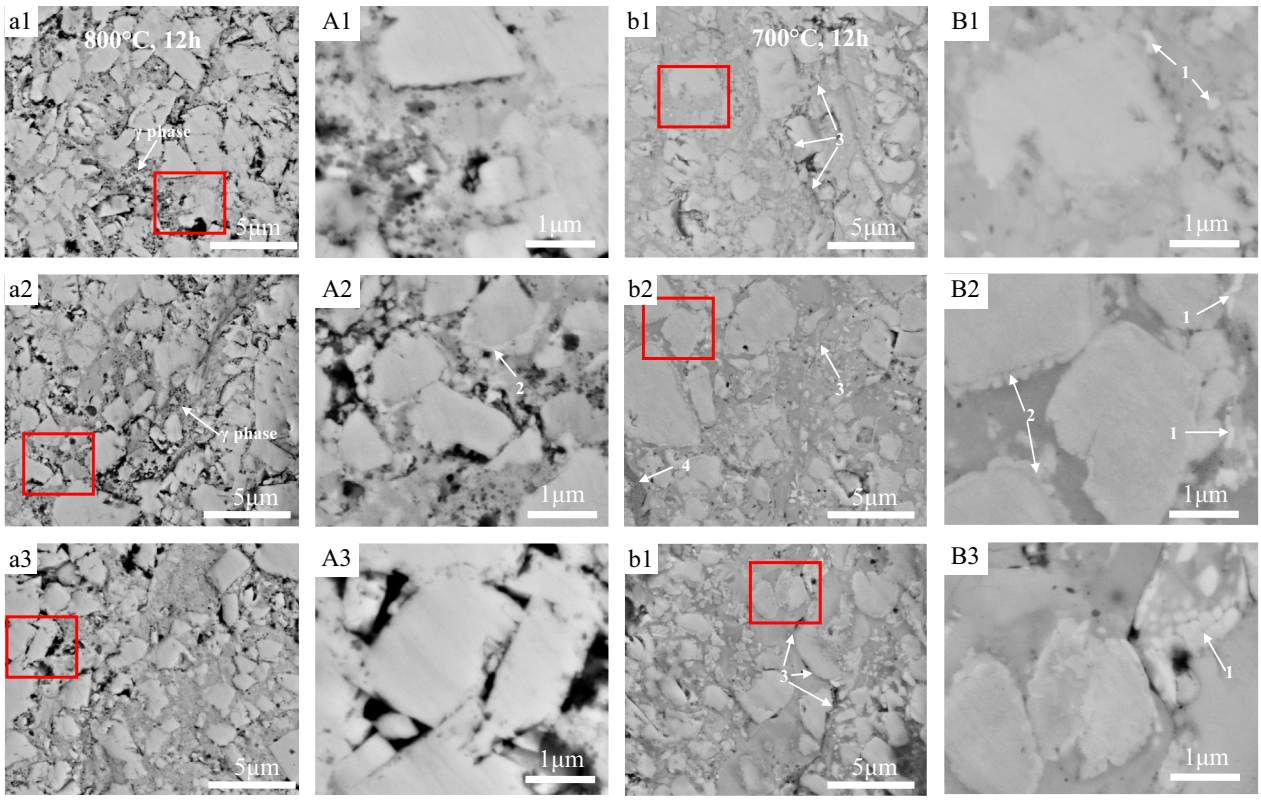

Fig. 7. Back Scattering Electron (BSE) images of the cross-section of samples deposited at (a) 800 °C in 12 h; (b) 700 °C in 12 h with different sites (1) near the steel substrate; (2) middle; (3) near the diamond film. The numbers represent 1: tungsten; 2: W_2C dendrites; 3: island boundary; and 4: Co aggregated area.

W_2C and $W_xCo_yC_z$. Even after 48 h deposition, these nano-sized phases distributed in the binder in the inner part of the coating. However, in the outer part of the interlayer, binder phases were transformed into WC completely. Overall, higher temperature is beneficial to the phase transformation of binder phase as well as carbon-poor phases in the coating. This conclusion is in accordance with the results reported by Kim [26], in which samples were processed by inert atmospheric heat treatment. But ordinary atmospheric heat treatment at high temperature (800 °C) will produce large-scale cracks [34] while they cannot be found when samples were treated using HFCVD.

$Co_3W_9C_4$ and Co_2W_4C will first transform into Co_3W_3C and W_2C. Then both Co_3W_3C and W_2C will react with the diffused carbon and produce WC. The reactions happened in the WC–Co coating during diamond deposition can be concluded as follows:

$$W_2C + C \rightarrow WC \quad (1)$$

$$Co_3W_9C_4 \rightarrow 3W_2C + Co_3W_3C \quad (2)$$

$$3Co_2W_4C + 2C \rightarrow 3W_2C + 2Co_3W_3C \quad (3)$$

$$Co_3W_3C + 2C \rightarrow WC + 3Co \quad (4)$$

4.2. Effect of depth on phase transition of WC–Co coating

As can be seen from the experimental results, the phase transition of coating not only related to temperature, but also closely connected to the depth of coating. After HFCVD, the WC–Co interlayer can be divided into three sections (i.e. near surface, near steel substrate and the middle part) because of the difference in phase evolution rate among these sections.

4.2.1. Near surface

From surface morphology of the samples (Figs. 1 and 2), Co nanoparticles were found on the surface diamond film. This is because Co in WC–Co interlayer evaporated under high temperature and low pressure condition. At high deposition temperatures, ball-shaped cobalt particles will form on the surface of the sample and can move during diamond deposition [35]. Also, when diamond film was depositing, a small fraction of Co on the surface of interlayer diffused to the surface of diamond through defects such as grain boundaries and cracks. The higher temperature will result in greater loss of Co because evaporation and diffusion process will be accelerated when temperature is high. As a result, the amount of binder phase dwindled and the distance between WC grains was reduced and the size of WC grain increased. The binder of outer part of interlayer has the fastest phase transition rate. On one hand, the evaporation of Co boosted the transformation of binder phase to WC. On the other hand, activated carbon atoms diffused into WC–Co coating, further facilitating the formation of WC.

The diffusion of cobalt increases the constraints in diamond coatings and decreases the quality of it. Therefore, the deposition temperature should be controlled in order to limit the diffusion and evaporation of cobalt during HFCVD. In addition, deposition time should not be too long. Otherwise, even under relatively low deposition temperature, the WC–Co interlayer will become brittle. For instance, near the surface of sample deposited at 700 °C for 48 h (Fig. 6(c3) and (C3)), the binder phase between each WC grain disappeared. Even though the surface hardness of the sample is large, other mechanical performances could be compromised because of the absence of binder phase.

4.2.2. Near steel substrate

The diffusion rate of Fe and Co is very large. Therefore, near steel substrate, Co in the binder phase will diffuse into steel

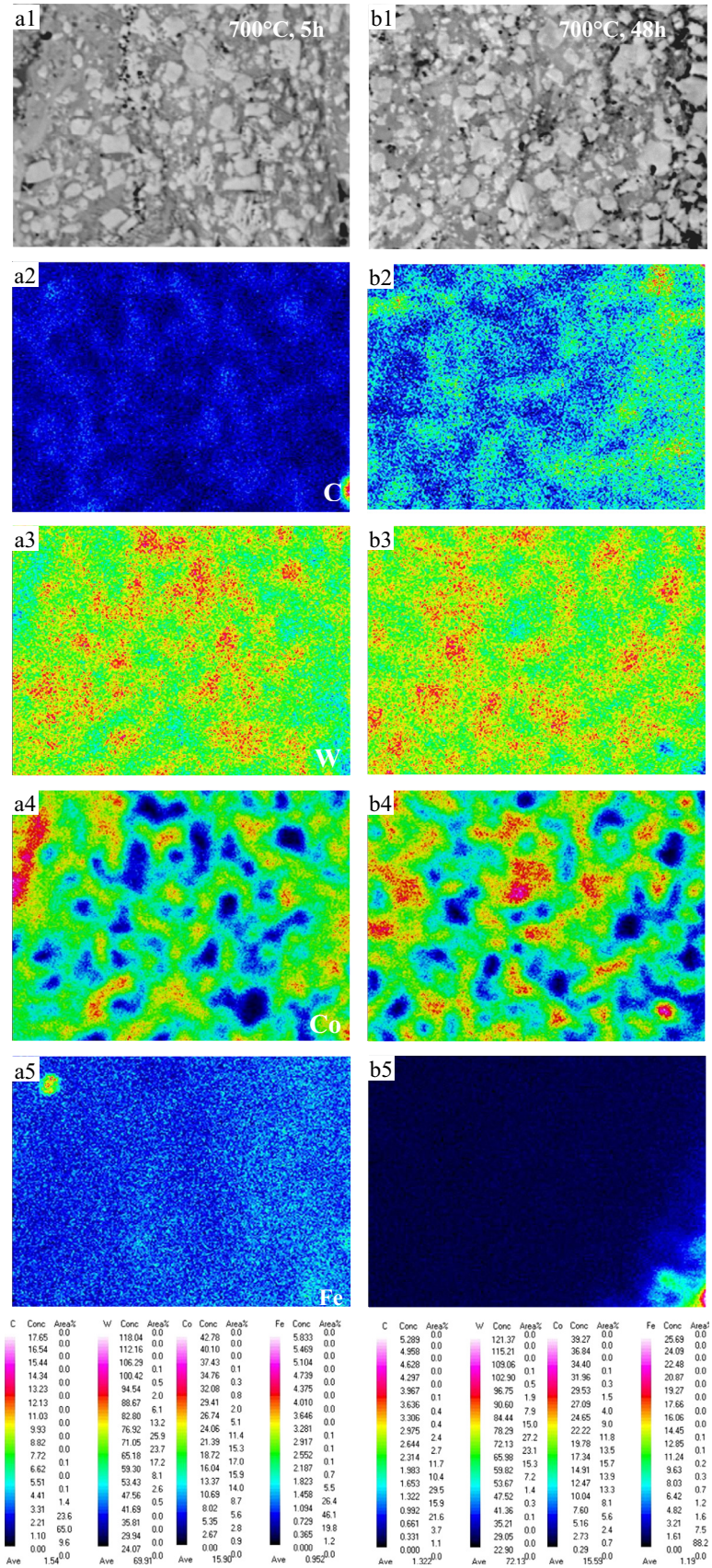

Fig. 8. EPMA images of the cross-section of samples deposited at 700 °C for (a) 5 h; (b) 48 h (1) BSE images; (2) carbon; (3) tungsten; (4) cobalt; and (5) iron.

substrate rapidly. Fe in steel substrate will also diffuse into WC–Co interlayer. Besides, the diffusion of Co boosted the transition of binder phase to WC. Therefore, we can find that near the substrate, the size of WC grain was larger and distance between WC grains was smaller. Compared with the outer part of the coating, the phase transition rate of binder phase was slower. The diffusion between Fe and Co can enhance the adhesion between WC–Co interlayer and steel substrate because of the chemical-bonded Co-Fe diffusion layer.

4.2.3. In the middle part

For the middle part of the interlayer, the diffusion and evaporation of Co was rather slow. Therefore, the phase transition rate of binder was the slowest and the average WC grain size was the smallest. The amount of W_2C was the largest. Therefore, the variation of elements in the coating was the main driving force of phase transition, while temperature plays an important role in the rate of element variation.

5. Conclusion

This paper investigated the effect of temperature on phase evolution of HVOF thermal spraying WC–Co coating during HFCVD and proposed a mechanism for phase transition. At high temperature, phase transition of binder phase was accelerated. After 5 h deposition, there is no amorphous phase and only small amount of W_2C remains in the coating. W_2C grains mainly distribute in the middle part of interlayer, on the rim of WC grain. WC grains in the surface and internal part of coating tend to aggregate and the grain size will be larger. Under lower temperature, phase transition becomes slower and a large amount of nano-phases will precipitate from the binder phase. In addition, it can be found that phase transition rate of binder is closely related to depth. Near the surface of WC–Co coating, Co will evaporate under high temperature and low-pressure condition and diffuse into diamond film. At the same time, activated carbon atoms will diffuse into the interlayer, but the diffusion depth is limited. At the interface between steel substrate and WC–Co coating, Fe and Co will diffuse into each other. However, diffusion will not occur in the middle part of WC–Co coating. Therefore, under the same deposition condition, the surface part of coating has the fastest phase transition rate, followed by the internal part of coating, while the middle part is the slowest. This demonstrates that near 700 °C and 800 °C, the main drive force of phase transition is the variation of elements in the coating, while temperature plays an important role in determining the rate of diffusion or evaporation.

Suitable substrate temperature and deposition time should be chosen before depositing diamond film on WC–Co coating. The deposition time should be controlled. If the deposition time is too long, the binder phase in the surface part of the WC–Co interlayer will vanish and the mechanical performance of the interlayer will be compromised. Temperature has great influence on the size and distribution of phases and grains. If substrate temperature is too high, the quality of diamond film will be reduced and the surface part of WC–Co interlayer will be brittle. Nevertheless, if temperature is too low, island boundaries in the coating will not disappear and there will be a large amount of nano-phase containing W, Co and C, which undermines the mechanical property of the coating.

Acknowledgements

We gratefully acknowledge the Nature Science Foundation of China (No. 51301211 & No. 21271188), the China Postdoctoral Science Special Foundation (No. 2014T70785), and the China Postdoctoral Science Foundation (No. 2012M521541) for financial support.

Appendix A. Supplementary material

Supplementary data associated with this article can be found, in the online version, at http://dx.doi.org/10.1016/j.jallcom.2015.03.134.

References

[1] H. Chen, M.L. Nielsen, C.J. Gold, R.O. Dillon, J. DiGregorio, T. Furtak, Growth of diamond films on stainless steel, Thin Solid Films 212 (1992) 169–172.
[2] K. Tsugawa, S. Kawaki, M. Ishihara, M. Hasegawa, Direct coating of nanocrystalline diamond on steel, Jpn. J. Appl. Phys. 51 (2012).
[3] Y.S. Li, T.J. Pan, Y. Tang, Q. Yang, A. Hirose, Selective synthesis of diamond and CNT nanostructures directly on stainless steel substrates, Diam. Relat. Mater. 20 (2011) 187–190.
[4] T. Liu, H. Pinto, P. Brito, L.A. Sales, D. Raabe, Residual stress analysis in chemical-vapor-deposition diamond films, Appl. Phys. Lett. 94 (2009) 201902.
[5] S.S. Shao, F.Z. Xuan, Z.D. Wang, S.T. Tu, Stress in film/substrate system due to diffusion and thermal misfit effects, J. Phys. D 42 (2009) 175413.
[6] Y.S. Li, A. Hirose, Direct coating of nanophase diamond films on steel substrate, Chem. Phys. Lett. 433 (2006) 150–153.
[7] V.F. Neto, R. Vaz, N. Ali, M.S.A. Oliveira, J. Grácio, Diamond coatings on 3D structured steel, Diam. Relat. Mater. 17 (2008) 1424–1428.
[8] J.P. Manaud, A. Poulon, S. Gomez, Y.L. Petitcorps, A comparative study of CrN, ZrN, NbN and TaN layers as cobalt diffusion barriers for CVD diamond deposition on WC–Co tools, Surf. Coat. Technol. 202 (2007) 222–231.
[9] J.G. Buijnsters, P. Shankar, W.J.P. van Enckevort, J.J. Schermer, J.J. Ter Meulen, The adhesion of hot-filament CVD diamond films on AISI type 316 austenitic stainless steel, Diam. Relat. Mater. 13 (2004) 848–857.
[10] J.G. Buijnsters, P. Shankar, W.J.P. van Enckevort, J.J. Schermer, J.J. Ter Meulen, The applicability of ultra thin silicon films as interlayers for CVD diamond deposition on steels, Phys. Status Solidi (a) 195 (2003) 383–395.
[11] F. Xu, J.H. Xu, M.F. Yuen, L. Zheng, W.Z. Lu, D.W. Zuo, Adhesion improvement of diamond coatings on cemented carbide with high cobalt content using PVD interlayer, Diam. Relat. Mater. 34 (2013) 70–75.
[12] V.F. Neto, T. Shokuhfar, M.S.A. Oliveira, J. Gracio, N. Ali, Polycrystalline diamond coatings on steel substrates, Int. J. Nanomanuf. 2 (2008) 99–115.
[13] V.G. Ralchenko, A.A. Smolin, V.G. Pereverzev, E.D. Obraztsova, K.G. Korotoushenko, V.I. Konov, Y.V. Lakhotkin, E.N. Loubnin, Diamond deposition on steel with CVD tungsten intermediate layer, Diam. Relat. Mater. 4 (1995) 754–758.
[14] J.G. Buijnsters, L. Vázquez, G. Van Dreumel, J. Ter Meulen, W. Van Enckevort, J.-P. Celis, Enhancement of the nucleation of smooth and dense nanocrystalline diamond films by using molybdenum seed layers, J. Appl. Phys. 108 (2010) 103514.
[15] Y.S. Li, H.T. Ma, L.Z. Yang, Q. Yang, A. Hirose, Enhanced diamond CVD synthesis on steel substrates modified by ion beam implantation and sputtering of Al, Surf. Coat. Technol. 207 (2012) 328–333.
[16] Y.S. Li, Y. Tang, Q. Yang, J. Maley, R. Sammynaiken, T. Regier, C. Xiao, A. Hirose, Ultrathin W–Al dual interlayer approach to depositing smooth and adherent nanocrystalline diamond films on stainless steel, ACS Appl. Mater. Interfaces 2 (2010) 335–338.
[17] Y.S. Li, Y. Tang, Q. Yang, C. Xiao, A. Hirose, Growth and adhesion failure of diamond thin films deposited on stainless steel with ultra-thin dual metal interlayers, Appl. Surf. Sci. 256 (2010) 7653–7657.
[18] Q. Wei, T. Yang, K. Zhou, L. Ma, P. Zheng, J. Li, D. Zhang, Z. Li, Z. Yu, Effect of sputtered Mo interlayers on Si (100) substrates for the deposition of diamond film by hot filament chemical vapor deposition, Surf. Coat. Technol. 232 (2013) 456–463.
[19] E. Hojman, R. Akhvlediani, A. Layyous, A. Hoffman, Diamond CVD film formation onto WC–Co substrates using a thermally nitrided Cr diffusion-barrier, Diam. Relat. Mater. 39 (2013) 65–72.
[20] Q.P. Wei, Z.M. Yu, L. Ma, D.F. Yin, J. Ye, The effects of temperature on nanocrystalline diamond films deposited on WC–13 wt.% Co substrate with W–C gradient layer, Appl. Surf. Sci. 256 (2009) 1322–1328.
[21] P. Suresh Babu, B. Basu, G. Sundararajan, Abrasive wear behavior of detonation sprayed WC–12Co coatings: influence of decarburization and abrasive characteristics, Wear 268 (2010) 1387–1399.
[22] R.J.K. Wood, Tribology of thermal sprayed WC–Co coatings, Int. J. Refract Metal Hard Mater. 28 (2010) 82–94.
[23] M.R. Thakare, J.A. Wharton, R.J.K. Wood, C. Menger, Investigation of micro-scale abrasion–corrosion of WC-based sintered hardmetal and sprayed coating using in situ electrochemical current-noise measurements, Wear 267 (2009) 1967–1977.
[24] M.M. Lima, C. Godoy, J.C. Avelar-Batista, P.J. Modenesi, Toughness evaluation of HVOF WC–Co coatings using non-linear regression analysis, Mater. Sci. Eng. A 357 (2003) 337–345.
[25] D.A. Stewart, P.H. Shipway, D.G. McCartney, Influence of heat treatment on the abrasive wear behaviour of HVOF sprayed WC–Co coatings, Surf. Coat. Technol. 105 (1998) 13–24.

[26] J.H. Kim, K.H. Baik, B.G. Seong, S.Y. Hwang, Effects of post-spraying heat treatment on wear resistance of WC–Co nanocomposite coatings, Mater. Sci. Eng. A 449–451 (2007) 876–879.
[27] F. Ghadami, S. Ghadami, H. Abdollah-Pour, Structural and oxidation behavior of atmospheric heat treated plasma sprayed WC–Co coatings, Vacuum 94 (2013) 64–68.
[28] D.A. Stewart, P.H. Shipway, D.G. McCartney, Microstructural evolution in thermally sprayed WC–Co coatings: comparison between nanocomposite and conventional starting powders, Acta Mater. 48 (2000) 1593–1604.
[29] C. Verdon, A. Karimi, J.-L. Martin, A study of high velocity oxy-fuel thermally sprayed tungsten carbide based coatings. Part 1: Microstructures, Mater. Sci. Eng. A 246 (1998) 11–24.
[30] J. Yuan, Q. Zhan, J. Huang, S. Ding, H. Li, Decarburization mechanisms of WC–Co during thermal spraying: insights from controlled carbon loss and microstructure characterization, Mater. Chem. Phys. 142 (2013) 165–171.
[31] Q. Wei, Z.M. Yu, M.N.R. Ashfold, Z. Chen, L. Wang, L. Ma, Effects of thickness and cycle parameters on fretting wear behavior of CVD diamond coatings on steel substrates, Surf. Coat. Technol. 205 (2010) 158–167.
[32] Q.-P. Wei, Z.M. Yu, M.N.R. Ashfold, L. Ma, Z. Chen, Fretting wear and electrochemical corrosion of well-adhered CVD diamond films deposited on steel substrates with a WC–Co interlayer, Diam. Relat. Mater. 19 (2010) 1144–1152.
[33] D.A. Stewart, P.H. Shipway, D.G. McCartney, Abrasive wear behaviour of conventional and nanocomposite HVOF-sprayed WC–Co coatings, Wear 225–229 (Part 2) (1999) 789–798.
[34] J.B. Donnet, D. Paulmier, H. Oulanti, T. Le Huu, Diffusion of cobalt in diamond films synthesized by combustion flame method, Carbon 42 (2004) 2215–2221.
[35] E. Hojman, R. Akhvlediani, E. Alagem, A. Hoffman, Cobalt out-diffusion and carbon phase composition at the WC–10%Co/diamond film interface investigated by XPS, SEM, Raman and SIMS, Phys. Status Solidi A 209 (2012) 1726–1731.